

PROBING THE RELATION BETWEEN FORCE—LIFETIME—AND CHEMISTRY IN SINGLE MOLECULAR BONDS

Evan Evans

*Physics and Pathology, University of British Columbia, Vancouver, Canada V6T 2A6;
Biomedical Engineering, Boston University, Boston, Massachusetts 02215;
e-mail: evans@physics.ubc.ca*

Key Words imaging the landscape of energy barriers in macromolecular bonds, strengths of single and multiple molecular bonds, dynamic force spectroscopy

■ **Abstract** On laboratory time scales, the energy landscape of a weak bond along a dissociation pathway is fully explored through Brownian-thermal excitations, and energy barriers become encoded in a dissociation time that varies with applied force. Probed with ramps of force over an enormous range of rates (force/time), this kinetic profile is transformed into a dynamic spectrum of bond rupture force as a function of loading rate. On a logarithmic scale in loading rate, the force spectrum provides an easy-to-read map of the prominent energy barriers traversed along the force-driven pathway and exposes the differences in energy between barriers. In this way, the method of dynamic force spectroscopy (DFS) is being used to probe the complex relation between force—lifetime—and chemistry in single molecular bonds. Most important, DFS probes the inner world of molecular interactions to reveal barriers that are difficult or impossible to detect in assays of near equilibrium dissociation but that determine bond lifetime and strength under rapid detachment. To use an ultrasensitive force probe as a spectroscopic tool, we need to understand the physics of bond dissociation under force, the impact of experimental technique on the measurement of detachment force (bond strength), the consequences of complex interactions in macromolecular bonds, and effects of multiply-bonded attachments.

CONTENTS

INTRODUCTION	106
Innovation of Dynamic Force Spectroscopy	106
GENERIC FEATURES OF TESTING BOND STRENGTHS WITH FORCE PROBES	108
Probe Mechanics	108
Testing Bond Strength	109
Loading Dynamics	109
Single Bond or Multiple Bonds?	111

SINGLE BOND KINETICS IN LIQUIDS UNDER EXTERNAL FORCE	111
Rate of Escape Over an Idealized Barrier Under Force	111
Rate of Unbinding in Complex Molecular Bonds	113
STOCHASTIC PROCESS OF BOND RUPTURE IN PROBE EXPERIMENTS	114
Rupture of a Simple Bond Under Dynamic Loading	114
Impact of Rebinding on Rupture Force and Role of Probe Mechanics	115
Impact of Soft-Polymer Linkages on Rupture Force	117
Dynamic Force Spectroscopy of Simple Bonds	118
Dynamic Force Spectroscopy of Complex Molecular Bonds	120
Force Spectra of Multiple Bonds	121
FINAL COMMENTS	125

INTRODUCTION

Weak noncovalent interactions govern structural cohesion and mediate many of life's functions in cells. Weak bonds and structures have limited lifetimes and so will dissociate under almost any level of force if pulled on for modest periods of time. Close to equilibrium in solution, large numbers of molecules continuously bond and dissociate under zero force, and application of a field to the reacting molecules simply reduces the ratio of bound-to-free constituents. But at infinite dilution, an isolated-single bond exists far from equilibrium and only has non-zero strength on time scales shorter than the time $t_{\text{off}} = 1/k_{\text{off}}$ needed for spontaneous dissociation. Pulled apart faster than t_{off} , a bond resists detachment. The detachment force can range up to—and even exceed—the adiabatic limit $f_{\infty} \sim |\partial E/\partial x|_{\text{max}}$ defined by the intermolecular potential $E(x)$ if the bond is broken in less time than required for diffusive relaxation (as done in molecular dynamics simulations; 19, 25, 29, 31). Therefore, the key to understanding measurements of bond strength lies in the relation between force—lifetime—chemistry at the molecular level.

Innovation of Dynamic Force Spectroscopy

On laboratory time scales, Brownian-thermal excitations fully explore the chemical energy landscape of a bond, and barriers along optimal pathways for dissociation determine bond lifetime. Under external force, barriers in the energy landscape are lowered and bond lifetime shortens. When isolated bonds are ruptured under steady ramps of force, barriers diminish in time and, thus, rupture force depends on rate of loading (= force/time). Measured over an enormous range of loading rates, the most frequent forces for failure plotted on a scale of log (loading rate) establish a dynamic spectrum of bond strength that images the prominent energy barriers traversed along the force-driven pathway (10, 13). In this way, the method of DFS probes the inner world of molecular interactions to reveal barriers that are difficult or impossible to detect in assays of near equilibrium dissociation. These inner barriers are the determinants of bond lifetime and strength under rapid detachment.

An important advance in single molecule methods, the DFS concept has been used to explore energy landscapes of biotin-(strept)avidin bonds (34), lipid anchoring in membranes (12, 30), carbohydrate-(selectin)protein bonds (11, 17), unfolding of Ig domains in the muscle protein titin (37) and in recombinant proteins (32), unfolding of FNIII domains in the extracellular matrix protein tenascin (36), cooperative unbinding of short DNA duplexes (46), homotypic bonds between cadherins (3), and even an attempt at covalent bonds (18). Because of the inherent exponential dependence of kinetic rates on barrier energies, the DFS method is most revealing when bonds are tested over many orders of magnitude in loading rate.

Although pioneering the study of molecular bond strength, most of the work before 1997 must be regarded as qualitative assays of bond failure because there was no systematic investigation of the dependence on time scale and because there was significant uncertainty in the numbers of bonds formed in probe-surface contact. Moreover, even when explored over a wide range of loading rates and certain that only single bonds are being tested, measurements of strength versus loading rate are vulnerable to subtle effects arising from probe mechanics and chemical linkage to the bond. So the objective of this chapter is not to give a detailed review of a burgeoning field, but rather to provide basic concepts and guidelines for how ultrasensitive force probes can be used as spectroscopic tools to help construct an accurate picture of bond chemistry. The focus is on probing the strengths of isolated bonds far from equilibrium, where energy barriers along the unbinding pathway create characteristic signatures in DFS. Where possible, important features are illustrated by key examples from the literature. The emphasis here is fundamentally different from the beautiful near-equilibrium studies of conformational transitions in homopolymers (33, 38) and DNA (8, 41), slow separation of strands in long DNA (9), plus other interesting elastic transitions in single DNA molecules (42–44). Likewise, although governed in many cases by similar far-from-equilibrium kinetics and a very exciting field of study, dynamics of molecular motors (e.g. 6, 16, 23, 24, 28, 35, 47) and mechanical enzymes (e.g. 21, 45, 49–51), are not discussed because of the dependence on chemical energy and the more complicated molecular mechanics involved in these actions.

At the outset, it is important to define the relevant length, force, and energy scales. These scales are quite familiar to single molecule experimenters but often not to other researchers. The length scale for molecular dimensions and interactions is obviously a nanometer ($\text{nm} = 10 \text{ \AA}$). One nanometer is comparable to spacing of molecules at a concentration of ~ 1 mole/liter and five hundred-fold smaller than wavelengths of visible light. In the case of force, weak noncovalent bonds break in the piconewton (pN) range. One piconewton is about one ten-billionth of a gram weight (10^{-10} gm) or ten thousand-fold smaller than what can be measured with an analytical microbalance. Together, the product of length and force scales provides the appropriate scale for energy—thermal energy $k_{\text{B}}T$ —which is ~ 4 pN \cdot nm at biological temperatures (~ 300 °K) or ~ 0.6 Kcal/mole for Avogadro's number ($\sim 6 \times 10^{23}$) of molecules.

GENERIC FEATURES OF TESTING BOND STRENGTHS WITH FORCE PROBES

Probe Mechanics

Most direct measurements of single bond strength have been performed with three types of ultrasensitive probes: the atomic force microscope (AFM) (5), where force is sensed by deflection of a thin silicon nitride cantilever; the biomembrane force probe (BFP) (15, 40), where force is sensed by axial displacement of a glass microsphere glued to the pole of a micropipet-pressurized membrane capsule; and the laser optical tweezer (LOT) (1, 1a, 2), where force is sensed by displacement of a microsphere trapped in a narrowly focused beam of laser light. Each of these probes acts as a very soft spring with a small elastic constant κ_f (increase in force Δf per deflection Δx) that ranges from <1 pN/nm to 1 nN/nm (also given in other units by $\text{pN/nm} = \text{mN/m} = \text{dyn/cm}$). Obviously, low values of probe stiffness represent high sensitivity to force for each nm deflection of the transducer. The subtle drawbacks of low stiffness are that the probe is susceptible to thermal fluctuations in position ($\delta x^2 \sim k_B T / \kappa_f$) and the response time t_f can be slow in an overdamped viscous-water environment. On the other hand, high probe stiffness results in large thermal fluctuations of the applied force ($\delta f^2 \sim k_B T \cdot \kappa_f$).

Little attention has been paid to hydrodynamic interactions, which can add significant forces to the probe when tests are performed at very high speeds in liquids. For example, quick application of a pulling force to the probe is retarded by viscous drag so that the tip deflection reports a smaller force than is actually applied. The hidden force is governed by the damping coefficient ζ of the probe and deflection speed v , i.e. $\zeta = f/v$. Difficult to predict accurately, the damping coefficient is essentially the product of a viscosity η for the liquid environment and a characteristic dimension L_ζ for the probe, i.e. $\zeta \approx \eta L_\zeta$. Thus, probe damping is expected to be of order $\zeta \sim 10^{-3}$ pN-sec/nm for an AFM, of order $\zeta \sim 10^{-4}$ pN-sec/nm for a BFP, and of order $\zeta \sim 10^{-5}$ pN-sec/nm for a particle trapped by LOT. With typical values of stiffness (10–100 pN/nm for AFM, 0.1–1 pN/nm for BFP and LOT), time scales for viscoelastic response of probes lie in the range $t_f = \zeta / \kappa_f \sim 10^{-5}$ – 10^{-3} sec. Hydrodynamic interactions also arise from rapid movement of the substrate relative to the probe and its tip. In AFM tests, the floor of the chamber is moved to/from contact with the tip so fluid is pushed past the cantilever and applies drag along the full length. Because the substrate is usually moved at fixed speed, the viscous force is constant and adds a bias to the cantilever deflection. Although similar in BFP tests, the flow past a BFP capsule and the drag are much lower because the moving substrates are small. Lastly, close proximity of the substrate to any of the probe tips leads to a hydrodynamic coupling that depends inversely on the separation between tip and substrate. When held together by a bond, there is little relative motion between tip and substrate so this coupling has minimal effect on the force experienced by the bond. But after bond rupture, the hydrodynamic coupling transiently retards probe

recovery as the substrate is retracted. Clearly, all of these hydrodynamic effects should be considered carefully in each force probe application.

Testing Bond Strength

With few exceptions, tests of bond strength with force probes follow a common approach. The tips and substrates are first decorated with reactive molecules using methods that vary from serendipitous physisorption to specific covalent attachment through heterobifunctional polymer spacers and attachment mediated by high-affinity noncovalent complexes such as biotin-streptavidin or monoclonal antibodies. Once prepared, the probe and substrate are repeatedly brought to/from contact by steady, precision movements. If decorated with a very low density of reactive sites, contact between the probe tip and the test surface will only produce an occasional bond. Under controlled conditions of contact, a low frequency of attachments in repeated trials provides quantitative verification of the likelihood of rare, single bond events (e.g. probability >0.9 when 1 attachment occurs out of 10 touches). When a rare bond has formed, the tip is held to the substrate during separation of the surfaces and the transducer is stretched. Bond rupture is signaled by rapid recoil of the transducer to its rest position with no intervening arrests. Rupture force is quantified by the maximum transducer extension. Histories of force over the course of approach—touch—separation with formation and rupture of a bond are demonstrated in Figures 1*a* and *b*. After hundreds of touches, the few detachment forces are cumulated into a histogram and the peak (most likely force for rupture) establishes the statistical measure of bond strength. Not well appreciated, bond forces—no matter how carefully measured or how precise the technique—are always spread in value, and the most frequent force depends on how fast the bonds are loaded. The subtle feature of the generic method is that the force experienced by an attachment is not constant but increases in time. This is important because thermally activated kinetics under rising force lead to a reciprocal relation between bond lifetime and rupture force. As shown by comparison of Figures 1*a* and 1*b*, bonds under slow loading have long lifetimes but only withstand small forces, whereas bonds under fast loading have shorter lifetimes and withstand larger forces. In this way, measurements of rupture force at many loading rates from very slow to extremely fast are used to explore the chemical energy landscape traversed in force-driven dissociation.

Loading Dynamics

Bond strength depends critically on how fast force is applied. With a linear spring attached directly to the bond, the loading rate r_f is constant for steady separation speed v_s as illustrated in Figures 1*a* and 1*b*. However, molecular structures connected to the bond play an important role in the rate of force application to the bond. Assuming that the bond is linked symmetrically to tip and substrate by components with a stiffness κ_m , the effective spring constant κ_s for coupling force to the bond is determined by the serial compliance $1/\kappa_s = 2/\kappa_m + 1/\kappa_f$. Further

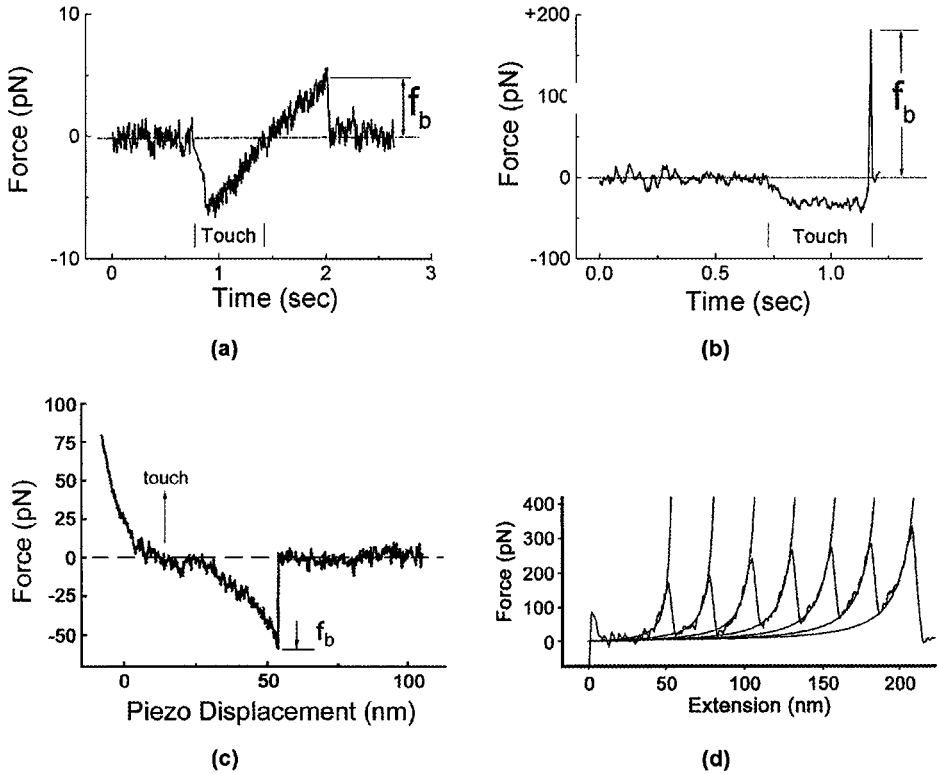


Figure 1 Rupture of single bonds with ultrasensitive force probes. (a, b) Steady loading of bonds with a biomembrane force probe BFP ($0.1 \text{ pN/nm} < \kappa_f < 3 \text{ pN/nm}$). Here, the micron-size glass tip of the BFP was decorated with a specific carbohydrate ligand and tested against a second glass microsphere decorated with a recombinant selectin receptor (as described in reference 11). (a) Moved toward the BFP tip, contact (touch) by the test particle was sensed at a force of $\sim 5 \text{ pN}$ and fed back to signal retraction of the test particle. Slow retraction exposed a bond that held the BFP tip to the test particle for $\sim 0.5 \text{ sec}$ and broke at $f_b \sim 5 \text{ pN}$ under a loading rate of $\sim 10 \text{ pN/sec}$. (b) Similarly moved to contact the BFP, a test particle was stopped, paused for $\sim 0.5 \text{ sec}$ after sensing a force of $\sim 30 \text{ pN}$, then retracted at high speed. Here, a bond held the tip to the surface for $\sim 0.003 \text{ sec}$ and broke at higher force $f_b \sim 180 \text{ pN}$ under the extremely fast loading rate of $\sim 60000 \text{ pN/sec}$. (c, d) Nonsteady loading of bonds through soft polymer linkages to stiff atomic force cantilevers AFM ($20 \text{ pN/nm} < \kappa_f < 1 \text{ nN/nm}$). (c) A substrate decorated with PEG-linked strands of short DNA was retracted after contact with an AFM tip decorated with complementary PEG-linked strands of DNA (taken from Strunz et al, 46). The formation of a duplex resulted in tensile forces (negative in the convention of AFM) that increased steeply as the linkage was stretched beyond 50 nm at a speed of 100 nm/sec . The asymptotic stiffening is consistent with the 30 nm lengths of the PEG chains. (d) The famous sawtooth pattern of force versus extension obtained from unfolding Ig domains in a recombinant construct of 8-Ig domains under constant pulling speed with an AFM (taken from Rief et al, 37). Each unfolding event produced a precipitous drop in force and added $\sim 30 \text{ nm}$ to the contour length. The curves superposed on each event are correlations with the worm-like chain model for polymer elasticity.

complications arise because most biomolecules and chemical linkers are highly flexible polymers with nonlinear elastic properties. First, these components are very soft, as revealed by the small thermal scale $k_B T / (L_p b)$ for stiffness of a polymer determined by contour length L_p and persistence length b . Thus, the stiffness scale is < 1 pN/nm even for relatively short linkers; and when connected to stiff probes like AFM cantilevers ($\kappa_f > 10$ pN/nm), the soft linkage dominates the effective spring constant (i.e. $\kappa_s \sim \kappa_m$). Second, we see in Figures 1c and 1d that bonds held by polymer-like connections experience highly nonlinear loading dynamics. Rupture occurs most often in the asymptotic regime ($x \rightarrow L_p$) of polymer stretch where force diverges as, $f \sim (k_B T / cb) / (1 - x/L_p)^\alpha$, with $\alpha = 1$ & $c = 1$ for a freely-jointed polymer and $\alpha = 2$ & $c = 4$ for a worm-like polymer. The loading rate under constant speed separation increases very rapidly as the polymer is pulled taut in time, $r_f(t) \approx (\alpha k_B T / c L_p b) v_s / (1 - v_s t / L_p)^{\alpha+1}$. We later see that this highly nonsteady loading can significantly affect the dependence of rupture force on detachment speed.

Single Bond or Multiple Bonds?

The principal concern in experiments is the number of bonds produced at each contact. Biomolecular structures bound to solid materials usually form compliant layers; so, the level of touching force determines the size of the contact area and the number of sites available for bonding. With a low density of sites and controlled impingement, the efficiency of bond recruitment over the duration of contact depends then on the mobility and lengths of linkages to the reactive sites. In addition, lateral fluctuations in probe position can increase bond recruitment over time for immobilized structures with short linkers. Thus, in order to use attachment frequency as a statistical estimator for rare single-bond events, each touch to the surface must have the same magnitude and history of contact force. This necessitates feedback control as demonstrated in Figures 1a and 1b. Even though rupture events only involve single molecular sites, it is still possible—and very likely under certain conditions—that a reactive pair of molecules may rupture and rebind many times before final separation. We later see that rebinding can significantly increase the level of detachment force.

SINGLE BOND KINETICS IN LIQUIDS UNDER EXTERNAL FORCE

Rate of Escape Over an Idealized Barrier Under Force

The connection between strength and lifetime of weakly bonded structures follows from the physics developed 60 years ago by Kramers (20, 27, 48) to describe overdamped kinetics of chemical reactions in condensed liquids. Starting far from equilibrium with all states confined local to a deep energy minimum, escape from a bound state is modelled as a constant diffusive flux of thermalized states

(Smoluchowski theory) along a preferential path over the confining barrier via a saddle point in the energy surface. There can be many such paths with tortuous trajectories in configuration space. However, application of an external field or force f acts to select a reaction path, which can then be represented by a scalar coordinate x . Analyzed along this coordinate, the outcome is a generic expression for escape or forward-transition rate k_{\rightarrow} that depends on how the energy landscape $E(x)$ is deformed under the applied field (10, 13),

$$k_{\rightarrow} = (D/l_c l_{ts}) \exp[-E_b(f)/k_B T]. \quad (1)$$

Neglecting many important aspects, the diffusive dynamics are embodied in the attempt frequency $D/l_c l_{ts}$, or diffusive relaxation time $t_D = l_c l_{ts}/D$, which is governed by molecular damping ($\zeta_m \equiv k_B T/D$) and two length scales. The first length l_c represents the thermal spread in bound states limited by the rise in energy $\Delta E_c(x)$ away from the minimum at x_c , i.e. $l_c = \int dx \cdot \exp[-\Delta E_c(x)/k_B T]$. The second length l_{ts} is the energy-weighted width of the barrier governed by the fall in energy, $\Delta E_{ts}(x)$, away from the transition state at the top of the barrier at x_{ts} , i.e. $l_{ts} = \int dx \cdot \exp[\Delta E_{ts}(x)/k_B T]$. With local harmonic approximations [e.g. $\Delta E_c(x) \approx \kappa_c (x - x_c)^2/2\dots$ and $\Delta E_{ts}(x) \approx -\kappa_{ts} (x - x_{ts})^2/2\dots$], these length scales are related to local curvatures, $\kappa = (\partial^2 E/\partial x^2)$, of the energy landscape by $l_c \approx (2\pi k_B T/\kappa_c)^{1/2}$ and $l_{ts} \approx (2\pi k_B T/\kappa_{ts})^{1/2}$.

The major impact of force stems from changes in the thermal likelihood of reaching the top of the energy barrier, i.e. $\exp[-E_b(f)/k_B T]$, where $E_b(f)$ describes the dependence of barrier height on applied force. In the most idealized view, the energy landscape is assumed to rise from the bound state and end with a sharp energy barrier. For a sharp barrier, the shape and location of the transition state are insensitive to force, but the barrier is lowered by force in proportion to the thermally averaged projection, $x_\beta = \langle x_{ts} \cos(\theta) \rangle$, of the barrier along the direction of force, i.e. $E_b(f) = E_b(0) - f x_\beta$, as sketched in Figure 2a. In this way, thermal activation sets the scale for force through the ratio of thermal energy to the distance x_β , i.e. $f_\beta = k_B T/x_\beta$, which can be surprisingly small since $k_B T \sim 4$ pN nm at room temperature and x_β can reach ~ 1 nm. On the scale f_β , rate of escape increases exponentially, $k_{\rightarrow} = (1/t_{\text{off}}) \exp(f/f_\beta)$, with force as first postulated by Bell (4) more than twenty years ago. But in contrast to the resonant frequency of bond excitations appearing in Bell's model, Kramers established that the attempt frequency for overdamped transitions in liquids is $1/t_D = (\kappa_c \kappa_{ts})^{1/2}/2\pi \zeta_m$, which is at least a thousand-fold slower. This attempt frequency drives thermally activated escape but the rate of escape is strongly discounted by the thermal unlikelihood of reaching the top of the barrier, which is the well known Arrhenius dependence on initial barrier height E_b . Thus, Kramers classic result for overdamped kinetics, $1/t_{\text{off}} = (1/t_D) \exp(-E_b/k_B T)$, sets the scale for escape rate at zero force. In liquids, kinetics of dissociation start with attempt frequencies of $\sim 10^9$ – 10^{10} /sec but end up at ~ 1 /sec for barrier heights of ~ 21 $k_B T$ or astonishingly at $\sim 1/40$ years for barrier heights of ~ 42 $k_B T$ and so on! Most important to note

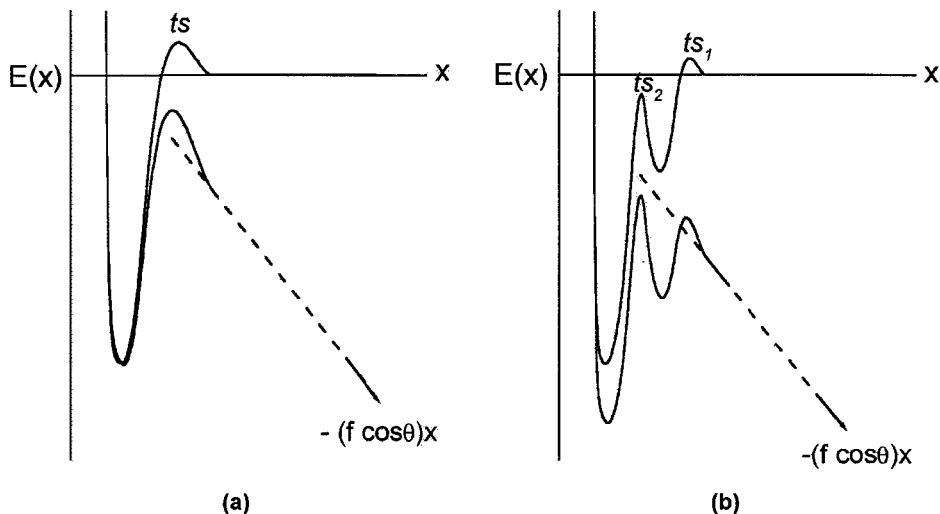


Figure 2 Conceptual energy landscapes for bonds confined by sharp activation barriers—transition states (*ts*). Oriented at an angle θ to the molecular coordinate x , external force f adds a mechanical potential $-(f \cdot \cos \theta)x$ that tilts the landscape and lowers barriers. (a) A single barrier under force. (b) A cascade of barriers under force where an inner barrier emerges to dominate kinetics when the outer barrier falls below by $\sim k_B T$.

is that the sharp barrier model—albeit naïve—captures the profound impact of thermally activated kinetics in bond rupture, i.e. the rate of failure rises exponentially once force reaches a small scale $k_B T/x_\beta$ well below the adiabatic limit $\sim E_b/x_\beta$!

Rate of Unbinding in Complex Molecular Bonds

In reality, macromolecular bonds involve many widely distributed atomic-scale interactions that can create a mountainous terrain of barriers in the energy landscape. When force is applied, outer barriers are driven below inner barriers so that an inner barrier then becomes the dominant impedance to unbinding as sketched in Figure 2*b*. This leads to a hierarchy of exponential amplifications in rate of escape under force (10). The transition rate for escape past a cascade of n sharp barriers is easily derived with Kramers' stationary-flux method. Implicit in this approach is the near equilibration of states over regions of the energy landscape below the principal barrier; states diffuse forward and back frequently over the lower barriers on the time scale for passage of the dominant barrier. The outcome is an unbinding rate governed by the sum of times needed to transit individual barriers starting from the bound state (10),

$$k_{\rightarrow} = 1/\sum_n t_{\text{off}}(n) \exp[-f/f_\beta(n)]. \quad (2)$$

Like a single barrier, the kinetic impedance of each n^{th} barrier in the hierarchy is described by a time for forward passage, $t_{\text{off}}(n) \approx t_{\text{D}} \exp[E_b(n)/k_{\text{B}}T]$, set by its height $E_b(n)$ above the bound state and a force scale $f_{\beta}(n) = k_{\text{B}}T/x_{\beta}(n)$ for rate exponentiation set by its projection $x_{\beta}(n)$ along the direction of force. At low force, the unbinding rate grows rapidly with the steepest exponential governed by the outermost barrier. At larger forces, the rate crosses over to more shallow exponentials defined by the inner barriers. We later see that this hierarchy of exponential scales for amplification does indeed characterize unbinding kinetics for complex biomolecular bonds under external force.

STOCHASTIC PROCESS OF BOND RUPTURE IN PROBE EXPERIMENTS

Rupture of a Simple Bond Under Dynamic Loading

Because of the enormous gap in time scale between diffusive relaxation ($t_{\text{D}} \sim 10^{-10}$ – 10^{-9} sec) and laboratory experiments ($\sim 10^{-4}$ sec to minutes), kinetic rates during bond rupture become continuous functions of the instantaneous force on the laboratory time scale. In the limit of large statistics, the distributions of rupture times and forces follow a first-order (*Markov*) process (48) where time and force are tied together through the loading dynamics. With no other constituents close enough to participate in binding, the master equation for evolution of an isolated pair of interacting molecules involves the net of unbinding (forward \rightarrow) and rebinding (reverse \leftarrow) transitions,

$$dS_1/dt = -k_{\rightarrow}(t)S_1(t) + k_{\leftarrow}(t)S_0(t), \quad (3)$$

where $S_1(t)$ is the likelihood of being in the bound state, and $S_0(t) \equiv 1 - S_1(t)$ is the likelihood of being detached. When pulled by an elastic linkage at constant speed, the loading dynamics are set by pulling speed v_s and the dependence of linkage stiffness $\kappa_s(f)$ on force, i.e. $df = [\kappa_s(f)v_s] dt$. Thus, the likelihood of bond survival can be described in terms of instantaneous force—now equivalent to time,

$$dS_1/df = -t_{\text{off}}[k_{\rightarrow}(f) + k_{\leftarrow}(f)]S_1(f)/r_f(f) + t_{\text{off}}k_{\leftarrow}(f)/r_f(f), \quad (4)$$

as expressed in dimensionless force $f = f/f_{\beta}$ and loading rate $r_f(f) \equiv t_{\text{off}}[\kappa_s(f)v_s]/f_{\beta}$.

The easiest rupture process to analyze is one where the disjoining force is persistent and does not diminish with separation distance (as illustrated in Figure 2). Once force rises above the thermal scale f_{β} , i.e. $\int r_f dt > t_{\text{off}}$, molecules separated well beyond the barrier continue to move apart faster than diffusion can recombine them and rebinding vanishes ($k_{\leftarrow} S_0 \sim 0$). Driven far from equilibrium, the kinetics of escape determine the likelihood of being in the bound state, i.e. $dS_1/df \approx - (t_{\text{off}} k_{\rightarrow}/r_f) S_1$ or equivalently $S_1(f) \approx \exp\{-\int_{0 \rightarrow f} [t_{\text{off}} k_{\rightarrow}(y)/r_f(y)] dy\}$.

The statistics of rupture between forces of f and $f + \Delta f$ are described by the distribution $p(f) \approx [k_{\leftarrow}(f)/r_f(f)] S_1(f)$. The distribution peak locates the force f^* for most frequent rupture, which defines bond strength. The peak arises from the crossover between exponentiation of failure rate and precipitous decline in bond survival under increasing force. The maximum, $\partial p(f)/\partial f = 0$, relates bond strength f^* to loading rate r_f through the expression,

$$[t_{\text{off}}k_{\leftarrow}]_{f=f^*} = r_f[\partial \ln(k_{\leftarrow})/\partial f - \partial \ln(r_f)/\partial f]_{f=f^*}. \quad (5)$$

Thus, far from equilibrium, a bond confined by a single-sharp barrier [where $t_{\text{off}}k_{\leftarrow} = \exp(f)$] fails most often at a force exactly proportional to $\log(\text{loading rate})$, i.e. $f^*/f_{\beta} = \ln(r_f)$, with a slope set by the thermal force f_{β} (10, 13). This simple relation shows that strength emerges when the loading rate becomes fast enough to contribute $k_B T$ of energy or greater to the bond within its natural lifetime t_{off} , i.e. $(\Delta f/\Delta t) \geq f_{\beta}/t_{\text{off}}$. Even with no experimental uncertainty, the distribution is broadened by kinetics and the standard deviation (Δ_f) is set by the thermal force, $\Delta_f = f_{\beta}$.

Impact of Rebinding on Rupture Force and Role of Probe Mechanics

As depicted in Figure 2, a persistent force tilts the energy landscape so that the bond exists far from equilibrium with little chance of rebinding after escape. In experiments, however, pulling on a bond with a probe creates a transient capture well that enables rebinding as illustrated in Figure 3a. The energy landscape only approaches the far-from-equilibrium condition if the probe linkage to the bond is very soft or once the force has become large enough to drop the energy level of the capture well below the bound state. For a harmonic disjoining potential, the ratio of rebinding-to-unbinding rates $k_{\leftarrow}/k_{\rightarrow}$ will diminish as $\sim \exp(-f^2/2\kappa_s)$ on a scale set by the dimensionless spring constant $\kappa_s \equiv \kappa_s x_{\beta}/f_{\beta}$ and force $f \equiv f/f_{\beta}$. In the context of Kramers' 1-D theory, on rate (1/time/concentration) is idealized by $k_{\text{on}} = (x_{\beta}/t_{\text{off}}) \exp[E_0/k_B T]$, where E_0 is the difference in energy between free and bound states. But when linked to a probe, the rate of rebinding can be retarded significantly so that we need to include the effect of probe-linkage dynamics in the kinetics. In addition, stiffness of the probe linkage (curvature of the potential) diminishes the reduction in barrier height under force and introduces a bias into the dependence of escape rate on force, i.e. $t_{\text{off}}k_{\rightarrow} = \exp(f - \kappa_s/2)$ for $f \geq \kappa_s$. This bias shows that the force must be large enough to push the capture well beyond the transition state to allow escape. [For extremely stiff probe linkages (> 1 nN/nm), the caveat is that the level of force $\kappa_s x_{\beta}$ may exceed the maximum gradient $|\partial E/\partial x|_{\text{max}}$ in the molecular potential of mean force. As such, thermal activation would not aid escape. Over the course of detachment, the probe force would reflect a thermally-weighted average of the gradient in free energy potential based on the variance in force, $\delta f^2 \sim k_B T \cdot \kappa_s$.]

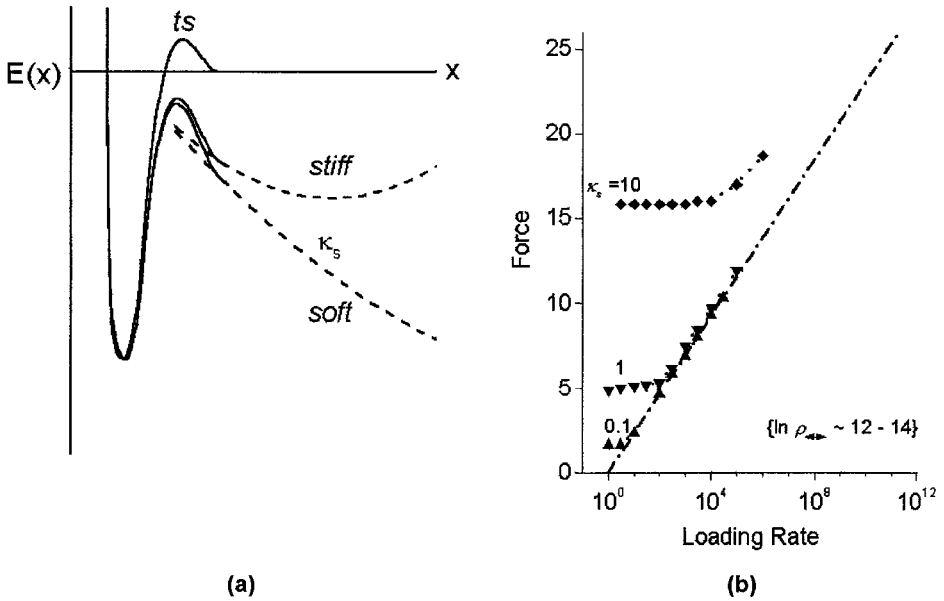


Figure 3 (a) Conceptual energy landscape for a simple bond under probe detachment. Elastic compliance of the probe linkage creates a transient capture well that enables rebinding and depends on stiffness κ_s . (b) Force thresholds for bond rupture produced at low rates of loading by rebinding as a function of probe linkage stiffness. Crossover to rate-dependent forces occurs when forward (escape) rate exceeds reverse (rebinding) rate, i.e. $k_{\rightarrow} > k_{\leftarrow}$, which depends on a characteristic ratio ρ_{\leftrightarrow} of dissociation-to-rebinding time scales (see text).

At the most simple level, rebinding is modelled by kinetics in two contiguous regions: The first region is the capture well, where viscous damping ζ_s and elasticity κ_s of the probe linkage govern relaxation time, i.e. $t_s \equiv \zeta_s/\kappa_s$. The second region is local to the barrier, where $t_{on} = x_\beta/k_{on}$ sets the time scale for entry to the bound state. Analyzed with Kramers' approach, the combined impedance of the two regions and the elastic potential yield the ratio of transition rates, $k_{\leftarrow}/k_{\rightarrow} \approx \rho_{\leftrightarrow} (\kappa_s/2\pi)^{1/2} \exp(-f^2/2\kappa_s)$, which depends on a pseudo-equilibrium constant, $\rho_{\leftrightarrow} = t_{off}/[t_{on} + t_s g(f)]$ with $g(f) \sim 1/f$ for $f > 1$. Based on this model and constant detachment speed, solutions of the master equation (Equation 4) demonstrate that rupture force remains close to a threshold until rebinding events vanish (i.e. once $k_{\rightarrow} > k_{\leftarrow}$ or $f > [2\kappa_s \ln(\rho_{\leftrightarrow})]^{1/2}$). We see in Figure 3b that the threshold depends strongly on stiffness of the probe linkage. Consequently, rebinding effects diminish when bonds are connected to probes by soft linkages like polymers. For example, consider freely jointed chains in the asymptotic regime; the ratio of transition rates is approximated by, $k_{\leftarrow}/k_{\rightarrow} \approx \rho_{\leftrightarrow} (\kappa_s/2\pi)^{1/2}/(f+1)^{Lp/b}$. (Again, $\rho_{\leftrightarrow} = t_{off}/[x_\beta/k_{on} + t_s g(f)]$ with $g(f) \sim 1/(f+1)$; the polymer is characterized by dimensionless stiffness, $\kappa_s \approx (x_\beta^2/L_p b)$, and damping ζ_s .) Because rebinding

vanishes when $k_{\rightarrow} > k_{\leftarrow}$, long polymers ($L_p/b \gg 1$) significantly suppress rebinding and the threshold drops to small forces approximated by $f \sim (\rho_{\leftrightarrow})^{b/L_p} - 1$.

Arising from transient confinement, the strength threshold is analogous to the close-to-equilibrium situation where depth of the disjoining potential matches the free energy of binding. However, in the case of bond breakage, the threshold regime may not represent unrestricted equilibrium; retardation by the probe linkage can lead to steady balances between unbinding and rebinding on a much longer time scale. Examining the rate-independent threshold and the crossover to a rate-dependent force could be a useful way to explore the approach to a bound state. On the other hand, accurate determination of barriers to dissociation requires that the rupture process be kept far from equilibrium, which reveals a special role for polymer linkages in the case of stiff probes.

Impact of Soft-Polymer Linkages on Rupture Force

Polymer linkages are very useful for projecting and isolating reactive sites in single-molecule experiments as well as for suppression of rebinding events. However, polymer linkages to stiff probes can introduce unexpected deviations in bond strength under steady speed detachment (14). Described earlier and demonstrated in Figures 1c and 1d, polymer connections produce nonlinear loading dynamics, where loading rate increases markedly near bond failure. For a stiff probe and constant detachment speed, the rate of loading increases with level of force, $r_f(f) \approx (v_s/v_\beta) f^{1+1/\alpha}$, parameterized by a characteristic velocity, $v_\beta \approx (L_p/\alpha t_{\text{off}})(x_\beta/cb)^{1/\alpha}$. (Recall: $\alpha = 1$ & $c = 1$ for a freely jointed polymer and $\alpha = 2$ & $c = 4$ for a worm-like polymer.) The thermal scale v_β for velocity represents the speed needed to pull the polymer taut within the time t_{off} for spontaneous unbinding. Hence, far from equilibrium, the most likely rupture force is derived from Equation 5 to be,

$$f^* \approx f_\beta \ln(v_s/v_\beta) + f_\beta [\ln(f^*/f_\beta - 1 - 1/\alpha) + (1/\alpha) \ln(f^*/f_\beta)], \quad (6)$$

which approaches the expected proportionality to $\log(\text{detachment rate})$ at high speeds ($v_s \gg v_\beta$) but deviates significantly at low speeds. Equation 6 shows that when pulled by polymers, measurements of rupture force versus separation velocity with stiff probes yield thermal scales for force f_β and velocity v_β but not the time scale t_{off} . In order to establish t_{off} , contour and persistence lengths (L_p , b) of the polymer linkage must be known. These features are demonstrated first in Figure 4a by correlation of Equation 6 to AFM tests of unfolding Ig domains in native titin, which yields $f_\beta \approx 12$ pN and $v_\beta \approx 6.7 \times 10^{-3}$ nm/sec. Taking $L_p \sim 100$ nm and $b \sim 0.4$ nm for the contour and persistence lengths of the titin worm-like chain (37), the approximate time scale for unfolding is $t_{\text{off}} \sim 1$ hr. Second in Figure 4b, correlation of Equation 6 to AFM tests of unbinding vascular endothelial (VE) cadherin dimers linked by PEG polymers (3) appears similar in form but yields very different values, $f_\beta \approx 5$ pN and $v_\beta \approx 8.3$ nm/sec. Taking a range of ~ 20 nm–60 nm reported (3) for the extended length L_p of the

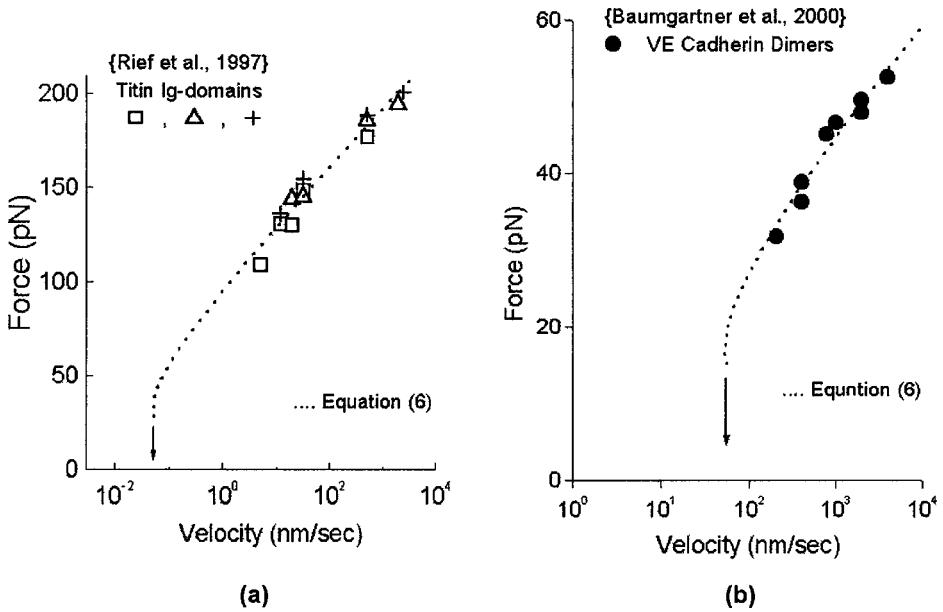


Figure 4 (a) Force versus log(velocity) obtained by unfolding Ig domains in ~ 100 nm pieces of native titin at steady speed with AFM (data replotted from Rief et al. 37). Matched to the data, the dotted curve is force as a function of pulling speed predicted by Equation 6 for asymptotic loading of a bond through worm-like polymers. (b) By comparison, lower forces were needed to rupture PEG-linked cadherin dimers with AFM under much faster speeds (data replotted from Baumgartner et al, 3). Matched to the data, the dotted curve is the prediction from Equation 6 for asymptotic loading of a bond through freely jointed polymers.

freely-jointed PEG (polyethyleneglycol) and $b \sim 0.4$ nm for segment length, the time scale for unbinding is, $t_{\text{off}} \sim 5\text{--}17$ sec. It is important to note that proper treatment of the polymer loading dynamics can lead to different barrier locations x_{β} and very different time scales t_{off} vis-a-vis those derived from straight line fits based on steady loading dynamics.

Dynamic Force Spectroscopy of Simple Bonds

Under steady ramps of force in time, the signature of escape over a sharp energy barrier is a straight line in a plot of rupture force versus log(loading rate). An example of this ideal behavior is shown in Figure 5a by BFP measurements of forces needed to extract single diC14 lipids from the surface of a lipid:cholesterol vesicle (12, 30). Linear in log(loading rate) over a thousand-fold span in rate, the slope f_{β} of the data in this case is governed by hydrophobic exposure of the lipid alkyl chains to water, which is ideally set by the insertion depth in the membrane. Thus, with ~ 2 nm for the half-thickness of a lipid:cholesterol membrane, the slope

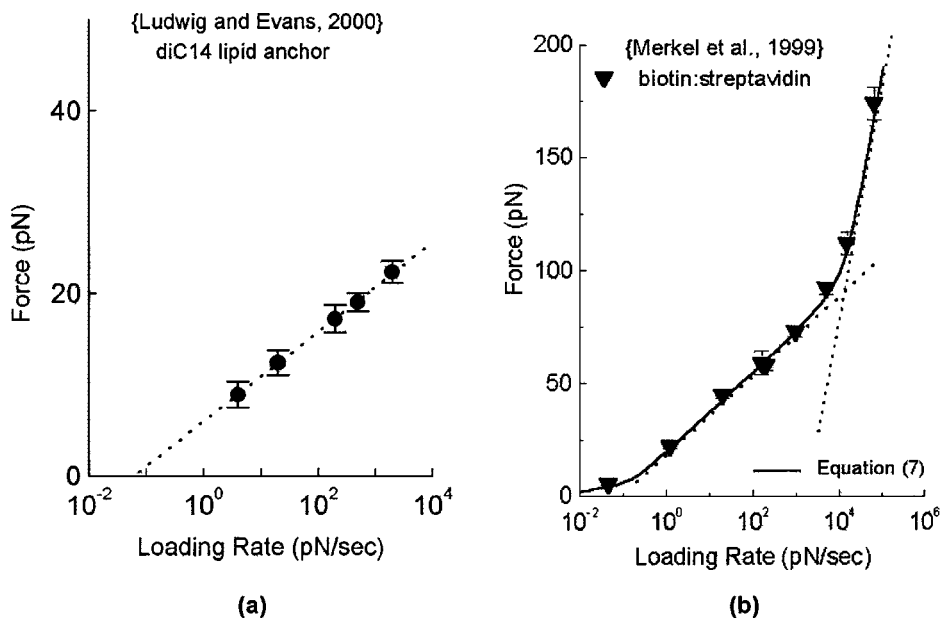


Figure 5 (a) Force versus log(loading rate) obtained by BFP extraction of single receptor lipids (biotin-PEG-diC14 PE) from a SOPC:CHOL lipid vesicle (12,30). (b) Force versus log(loading rate) obtained by BFP rupture of single biotin bonds to streptavidin (34). Matched to the data, the solid curve shows the continuous spectrum predicted by Equation 7 for passage of two energy barriers. The dotted lines show the linear spectra of force proportional to log(loading rate) that each barrier would produce independently set by its thermal scale for force $f_\beta = k_B T/x_\beta$ and rate of transition $1/t_{\text{off}}$.

of strength versus log(loading rate) is expected to be $\sim k_B T/2$ nm, which is close to the slope ~ 2.1 pN of the data in Figure 5a. The loading rate $(\Delta f/\Delta t)_{f^*=0}$ extrapolated to zero force and the slope f_β establish an apparent force-free lifetime, i.e. $t_{\text{off}} \approx f_\beta/(\Delta f/\Delta t)_{f^*=0}$, which is ~ 30 seconds for diC14 lipid anchoring. Together, the thermal scales for force and apparent lifetime define the kinetics of lipid unbinding as a function of pulling force, which is a single exponential in this case. The outcome reveals the profound impact of force on the rate of lipid unbinding, which increased from an apparent force-free off rate of $\sim 0.03/\text{sec}$ to $> 1500/\text{sec}$ at small forces of ~ 23 pN.

The off rate $1/t_{\text{off}}$ obtained from extrapolation of lipid pullout to zero force is labelled apparent because the value is fifty-fold faster than the rate for dissociation of similar PEG-biotinylated diC14 lipids from lipid vesicles in solution (39). The slower rate in solution implies that lipids stick transiently to a membrane interface—albeit weakly—after leaving the hydrocarbon core. This comparison demonstrates that molecular attractions exterior to a binding site can significantly prolong association in solution yet escape detection in probe tests because the

peripheral interaction is overwhelmed by small forces (e.g. ≤ 1 pN). Likewise, application of force could also eliminate pathways available to spontaneous dissociation, which would yield a slower apparent off rate. Hence, there is no reason to expect that the apparent lifetime derived from extrapolation of rupture kinetics to zero force should match the lifetime measured for dissociation in solution.

Very useful, however, the logarithmic intercept $\ln(\Delta f/\Delta t)_{f^*=0}$ is governed by height of the barrier, i.e. $\ln(\Delta f/\Delta t)_{f^*=0} = -E_b/k_B T + \ln(f_\beta/t_D)$, relative to a logarithmic bias set by the molecular scale f_β/t_D for loading rate. Hence, changes in the intercept and slope of a linear regime can be used to quantify chemical modifications of barrier energy, i.e. $\Delta E_b/k_B T \approx -\Delta \ln(\Delta f/\Delta t)_{f^*=0} + \Delta \ln(f_\beta)$, assuming that molecular damping remains constant. With location x_β of a transition state implicit in the slope and barrier energy linked to loading rate intercept, linear proportionality of force to $\log(\text{loading rate})$ provides a dynamic-spectral image of a single activation barrier.

Dynamic Force Spectroscopy of Complex Molecular Bonds

Rupture of a complex molecular bond is likely to involve passage over a cascade of activation barriers. As described earlier, application of force leads to suppression of outer barriers and exposure of inner barriers, which then dominate kinetics (cf. Figure 2*b*). Because force increases with time, the nontrivial aspect of a complex bond is that the flux of states can vary significantly over the energy landscape where the local minima between barriers may act as transient “attractors” for states. In this situation, a hierarchy of master equations (Table 1) must be solved to describe transitions from the bound state to the next local minimum and so on until reaching the final detached state, where likelihood of being in the N^{th} level (local minimum) is the function $S_N(t)$ of time. Under the rising force, the forward transition rates $k_{N \rightarrow N-1}$ and ratios of forward-to-reverse rates ($k_{N \rightarrow N-1}/k_{N \leftarrow N-1}$) evolve as $\exp[f(t)/f_\beta(N)]$ and $\exp(-\Delta E_{N,N+1}(t)/k_B T)$ driven by time-dependent changes in force. Although rapid dynamics can be very complicated (20), the simplifying feature for barriers separated by large differences in energy is that a prominent barrier, exposed by the instantaneous level of force, effectively limits the diffusive trickle of states leading to rupture at a particular time. Thus, the rate of escape can be approximated by the reciprocal sum of times to transit barriers expressed in Equation 2 but where force now depends on time. Under a ramp of force, rupture of a complex bond is thereby reduced to escape over a single-dynamic barrier that changes location along the reaction coordinate as well as height with time. (Far from equilibrium, solution of the master equations for dissociation at constant force yields exactly the result given by Equation 2.)

With the time-dependent unbinding rate approximated by Equation 2, the most frequent force f^* for detachment of a complex bond is easily derived from Equation 5 and follows a transcendental dependence on loading rate $\Delta f/\Delta t$ given by,

$$\sum_n [t_{\text{off}}(n)/f_\beta(n)] \exp[-f^*/f_\beta(n)] = 1/(\Delta f/\Delta t). \quad (7)$$

TABLE 1 Master equations for evolution of states in an N-level system

<i>Bound</i>
⋮
⋮
$dS_N/dt = -\{k_{N \rightarrow N-1} + k_{N+1 \leftarrow N}\} S_N(t) + k_{N+1 \rightarrow N} S_{N+1}(t) + k_{N \leftarrow N-1} S_{N-1}(t)$
⋮
⋮
<i>Unbound</i>
$dS_0/dt = -k_{1 \leftarrow 0} S_0(t) + k_{1 \rightarrow 0} S_1(t)$

[Again, each n^{th} barrier is described by a time scale for passage $t_{\text{off}}(n) \approx t_D \exp[E_b(n)/k_B T]$ set by the height $E_b(n)$ above the bound state and a force scale $f_\beta(n) = k_B T/x_\beta(n)$ set by the length $x_\beta(n)$.] The continuous nature of this spectrum is demonstrated in Figure 5*b* by correlation to BFP detachment of biotin-streptavidin bonds (34). The analytical spectrum for multiple barriers crosses over smoothly from one near-linear regime to the next, connected by a high-curvature bend. The dashed lines in Figure 5*b* show the linear functions of $\log(\text{force}/\text{time})$ defined by the transition rate $1/t_{\text{off}}(n)$ and force $f_\beta(n)$ derived for each barrier from the correlation. We then see that throughout each regime, a single activation barrier or chemical transition state dominates unbinding kinetics. In Figure 5*b*, the strength regimes for biotin-streptavidin place the first barrier at $x_\beta \sim 0.1$ nm and the next barrier at $x_\beta \sim 0.5$ nm. These two transition states are consistent with the effective locations of prominent chemical barriers revealed by molecular dynamics (19, 22) in simulations of biotin-streptavidin rupture (when averaged over rapid motions; 10, 13). Though difficult to access, another low strength regime seems to characterize very long time scales at forces below 5 pN (34). Relative to the off rate of $\sim 1/55$ hrs in solution, the rate of unbinding for biotin-streptavidin bonds increases dramatically in these experiments, first to $\sim 1/\text{min}$ under minuscule forces of ~ 5 pN, and ultimately to $\sim 3000/\text{sec}$ as force reaches 200 pN—almost nine orders of magnitude amplification! The power of DFS is the capability to look inside molecular interactions and accurately determine properties of prominent transition states that govern this incredible reduction in lifetime. Moreover, the prominent barriers imaged by DFS along the force-driven reaction coordinate provide important data for comparison with molecular dynamics simulations to provide new insights into molecular chemistry (10, 22, 29). However, the challenge is to measure forces over many orders of magnitude in loading rates.

Force Spectra of Multiple Bonds

A major complication in measurements of bond strength is the occurrence of multiple bonds. Moreover, single attachments between macromolecules often involve binding interactions distributed over many widely separated groups and behave as multiply bonded systems. Even if the numbers of bonds or localized sites for

binding are known, force spectra for multiply bonded structures can be difficult or impossible to interpret because the partition of force and the degree of cooperativity among binding sites are unknown. However, force spectra for a few generic types of multiple bonds can provide useful insights into the nature of hidden interactions in a molecular assembly. We begin with a description of mechanical scenarios for these multiple bonds. In the case of bonds in series, force is experienced fully by each bond. By comparison, a zipper is an array of bonds where force is applied only to the lead bond; once that bond fails, force propagates to the next bond and so on. Finally, for bonds in parallel, the force is partitioned among existing bonds in the attachment. These idealized cases are simple stereotypes of multiply bonded attachments. It is important to recognize that structural deformation on the nanoscale can lead to very different conditions of loading for multiple bonds. Still, the series, zipper, and parallel bond descriptions encompass a broad range of configurations.

For complete cooperativity, the series and parallel loading cases are simple. The bonds act as a macro-single bond with a barrier given by the sum of individual barrier energies. When N -identical bonds are considered, the time scale for dissociation rises exponentially as approximated by $t_{\text{off}}(N) \approx N t_{\text{off}} \exp[(N-1)E_b/k_B T]$. (The prefactor N is based on the putative model that molecular damping also scales with N .) For identical bonds in parallel, location of the transition state and thermal force scale remain that for a single bond, i.e. $f = f/f_\beta$. However, for identical bonds in series, each bond contributes an increment in length along the direction of force in unbinding, and thus, the thermal force scale is reduced N -fold, i.e. $f = N f/f_\beta$. The unbinding rate for N bonds in series, $t_{\text{off}}(N) k_{\rightarrow} = \exp(Nf)$, increases much faster with force than the rate for N bonds in parallel, $t_{\text{off}}(N) k_{\rightarrow} = \exp(f)$. As such, it takes much less force for cooperative failure of N bonds in series far from equilibrium, i.e.

$$f^* \approx (f_\beta/N)[\ln(r_f) + 2 \ln(N) + (N-1)E_b/k_B T], \quad (8)$$

than for N bonds in parallel, i.e.

$$f^* \approx f_\beta[\ln(r_f) + \ln(N) + (N-1)E_b/k_B T], \quad (9)$$

as derived with Equation 5. An important corollary for cooperative failure of N bonds in series is that the width of the force distribution narrows as $1/N$, i.e. standard deviation $\Delta_f = f_\beta/N$, which is to be expected.

Cooperative unbinding of N bonds in series has been beautifully demonstrated by AFM fracture of short DNA duplexes (46). In Figure 6a, the forces needed to fracture duplexes as a function of detachment speed are shown correlated with Equation 8. Each force spectrum follows the form given in Equation 6 because PEG polymers were used as linkages for the complementary strands (46). Thus, the correlation in Figure 6a yields thermal scales for force $f_\beta/N \sim (35/N)$ pN (i.e. $x_\beta \sim N \times 0.116$ nm) and velocity, $v_\beta(N) \sim (3 \times 10^5 \text{ nm/sec}) \exp[-(N-1)E_b/k_B T]$, characterized by an energy per base pair $E_b \sim 1.4 k_B T$. To derive the

apparent lifetime $t_{\text{off}}(N)$ for each duplex, the contour length L_p and persistence length b of the polymer linkage must be specified, i.e. $t_{\text{off}}(N) \approx (1/N)[L_p/v_\beta(N)] [x_\beta(N)/b]$. Figure 1c taken from the report (46) indicates that the contour length for the PEG linkers is approximately $L_p \sim 60$ nm with a segment length $b \sim 0.4$ nm. Thus, the apparent lifetime for a duplex increases exponentially with the number of base pairs as, $t_{\text{off}}(N) \approx (10^{-5} \times 10^{0.6N})$ sec. The decrease of force scale and exponentiation of time scale with number of base pairs were nicely demonstrated in the report (46). However, more explicit treatment of the nonlinear loading dynamics in Figure 6a yields a much faster time scale for kinetics than was obtained from straight line fits and steady loading dynamics based on a fixed estimate for polymer stiffness.

Random, uncooperative failure leads to a completely different behavior for multiply bonded attachments. The trivial case is that of N -identical bonds in series. Here, each bond experiences the same force history and any rupture event leads to failure of the attachment. Thus, when driven far from equilibrium, the rate of failure events is N -fold faster than the rate for one bond, which weakens the attachment slightly compared to a single bond at a particular loading rate, i.e. $f^* = f_\beta [\ln(r_f) - \ln(N)]$. More subtle, we expect a linkage of dissimilar bonds to rupture most often at the weakest bond and naïvely also expect that strong versus weak should scale as the energy barriers sustaining the bonds. But surprisingly, thermal force scales for exponentiation of unbinding rates are also important factors in determination of strong versus weak. This follows from the failure rate given by the sum of unbinding rates for the bonds. Taking properties (t_{off} or E_b , and f_β) of the bond with smaller barrier energy for a reference, the rate of failure for two bonds in series is expressed as, $t_{\text{off}} k_{\rightarrow} \approx \exp(f/f_\beta) \{1 + \exp[-\Delta E_b/k_B T + f \Delta(1/f_\beta)]\}$; $\Delta E_b > 0$ and $\Delta(1/f_\beta)$ are the differences of barrier energy and rate-exponentiation scale for the bond with the higher barrier. Based on the combined rate of failure, the force spectrum derived from Equation 5 shows that the bond with the smaller energy barrier will remain the weak bond so long as the inequality, $\Delta E_b/k_B T > f \Delta(1/f_\beta)$, holds. This means that the bond with a small barrier always unbinds faster [i.e. $\Delta(1/f_\beta) < 0$ or equivalently $\Delta(x_\beta) > 0$]. However, if the bond with a higher barrier has a greater amplification of rate under force [i.e. $\Delta(1/f_\beta) > 0$], then a crossover, $\Delta E_b/k_B T < f \Delta(1/f_\beta)$, will occur as the force is increased. Beyond the crossover, the bond with a higher barrier will become the most likely site of failure (i.e. the weak bond). Thus, in a DFS spectrum, an abrupt reduction of slope from a linear regime at low loading rates to the next linear regime at higher rates signals a switch in site for failure among bonds in a series linkage (10).

In zipper-like failure, bonds break in sequence at random times from first to last. As such, the master equations in Table 1 predict the likely sequence of rupture events where each bond along the zipper acts like a barrier in a complex bond, and the index “ n ” ranges over the number of bonds, i.e. $N \geq n \geq 1$. Hence, far from equilibrium, the single-dynamic barrier model expressed by Equations 2 and 7 can be used to approximate the detachment force under steady loading. Given identical bonds, $t_{\text{off}} k_{\rightarrow} \approx 1/[\sum_n n \exp(-f)] = \exp(f)/N$, so final separation

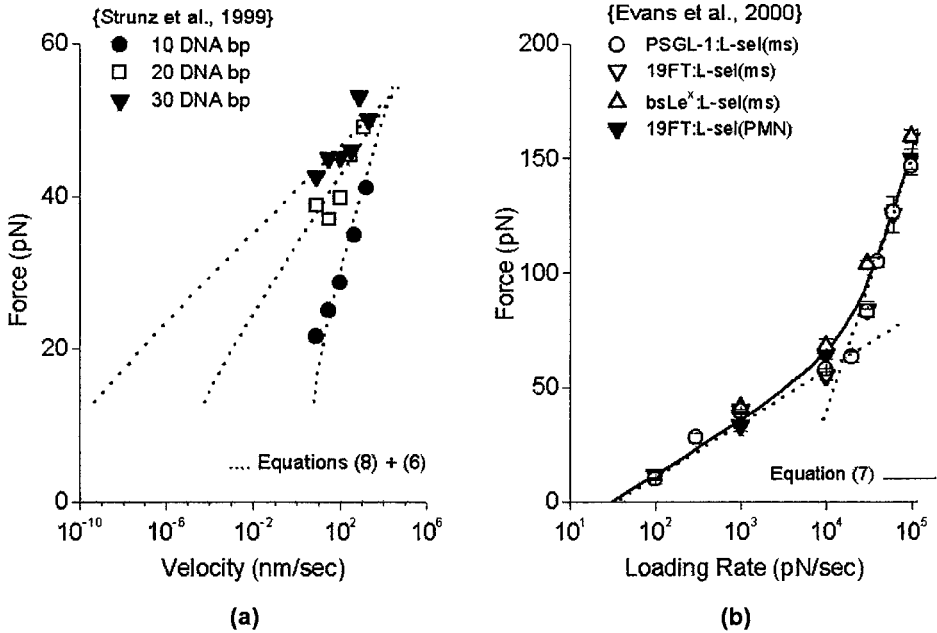


Figure 6 (a) Force versus $\log(\text{velocity})$ obtained by fracture of PEG-linked duplexes of DNA at steady speed with AFM (data replotted from Strunz et al, 46). The slopes of the data diminish with increase in number of base pairs, which led to the conclusion that the unbinding process was cooperative (46). Matched to the data, the dotted curves are forces as a function of pulling speed predicted by the cooperative model in Equation 8 using Equation 6 to represent loading of the duplexes through freely jointed polymers. (b) Force versus $\log(\text{loading rate})$ obtained by BFP rupture of single carbohydrate ligand bonds to L-selectin (11). The ligands represent important functional components of the mucin P-selectin glycoprotein ligand-1: the native homodimer (PSGL-1), an Ig chimera of the 19 amino acid tip of PSGL-1 (19FT), and the tetrasaccharide sialyl Lewis^X (bsLe^X). Both native L-selectin on leukocytes (PMN) and recombinant L-selectin on glass microspheres (ms) were probed with the ligand-decorated BFP. Matched to the data, the solid curve shows the continuous spectrum predicted by Equation 7 for passage of two energy barriers. The dotted lines show the force proportional to $\log(\text{loading rate})$ spectrum that each barrier would produce independently.

of the zipper occurs at a force, $f^* = f_\beta [\ln(r_f) + \ln(N)]$, only slightly larger than needed to break the lead bond. This feature is seen in multiple unfolding of Ig domains along native titin by LOT (26). On the other hand, macromolecular zippers are made up of widely separated and chemically diverse bonds. A good example is the complex carbohydrate-protein bond formed between the mucin P-selectin glycoprotein ligand-1 (PSGL-1) and the lectin domain of a selectin receptor. In Figure 6b, force spectra are shown for detachment of PSGL-1 bonds (and small molecular components of PSGL-1) to L-selectin (11). Surprisingly, strengths of bonds between the small tetrasaccharide sLe^X and L-selectin are nearly

indistinguishable from strengths of L-selectin bonds to the native 316 amino acid PSGL-1 or its outer 19 amino acid tip (which has one site for sLe^X) over almost four orders of magnitude in loading rate. The spectra reveal a sequence of two transition states. As found by correlation with Equation 7 in Figure 6*b*, slopes of the two strength regimes place the first barrier at $x_\beta < 0.1$ nm and the next barrier at $x_\beta \approx 0.4$ nm. When EDTA was added to chelate Ca⁺⁺, the high strength regime vanished and, thus, the transition state was shown to originate specifically from a Ca⁺⁺ bond between a single sLe^X group and the lectin domain (11). This demonstrates how DFS can be used to identify unique arrangements of small molecules that govern bond strength on different time scales.

Finishing with identical bonds loaded in parallel, we assume that each bond rupture event is far from equilibrium with no chance of rebinding and that force is shared equally by existing bonds in the attachment. Thus, the force experienced by bonds increases with each failure event during detachment, i.e. $f/\text{bond} = f/(N - n)$ with n from $0 \rightarrow N - 1$. Also, at each step, there are $N - n$ possibilities for unbinding, which decreases the time scale for events by $1/(N - n)$. With these rules for load distribution and time scale, rupture of N -bonds in parallel under constant rate of loading can again be modeled far from equilibrium with Equations 2 and 7. As such, the unbinding rate, $t_{\text{off}} k_{\rightarrow} = 1/\{\sum_{1 \rightarrow N} (1/n) \exp(-f/n)\}$, is roughly approximated by, $t_{\text{off}} k_{\rightarrow} \approx (f/N) \exp(f/N)$, which implies that forces needed to break a parallel bond attachment are essentially a factor of N larger than for a single bond under the same rate of loading,

$$f^* \approx N f_\beta [\ln(r_f) - \ln(f^*/f_\beta)]. \quad (10)$$

As a final note regarding these multiple bond models, numerical solutions to the master equations yield nearly the same detachment forces as those predicted by collapse of the N -level hierarchy to a single-dynamic barrier when driven far from equilibrium. This demonstrates the efficacy of the approximation expressed by Equations 2 and 7.

FINAL COMMENTS

We have seen that measuring the relation between force and lifetime can provide an intimate view of prominent barriers in the chemical energy landscape that govern physical strength and kinetics of molecular bonds under stress. At the same time, specific experimental requirements must be met to obtain a reliable picture of this landscape. Not only do we need an accurate and sensitive force probe, we first have to be confident that we are only testing single molecular attachments. This means we have to operate with extremely dilute sites for attachments, and we must also regulate the assembly process (e.g. through very soft touch under feedback control). Next, we have to know the compliance properties of the linkage to the bond (e.g. the contour and persistence lengths of polymeric connections) and the dynamic response when coupled to the probe. Having met these requirements, it

is imperative to measure forces over an enormous range of time scales or, more specifically, loading rates. As shown by the force spectra for ligand-receptor bonds, measuring forces over two orders of magnitude or less in rate, as done in many probe experiments, only provides a narrow glimpse of the landscape and can completely miss important features of complex chemical interactions.

ACKNOWLEDGMENTS

The author gratefully acknowledges support from US National Institutes of Health grants HL31579 and HL54700 and from Medical Research Council of Canada grant MT7477.

Visit the Annual Reviews home page at www.AnnualReviews.org

LITERATURE CITED

1. Ashkin A. 1992. Forces of a single-beam gradient laser trap on a dielectric sphere in the ray optics regime. *Biophys. J.* 61:569–82
- 1a. Ashkin A. 1997. Optical trapping and manipulation of neutral particles using lasers. *Proc. Natl. Acad. Sci. USA* 94:4853–60
2. Ashkin A, Schutze K, Dziedzic JM, Euteneuer U, Schliwa M. 1990. Force generation of organelle transport measured in vivo by an infrared laser trap. *Nature* 348:346–48
3. Baumgartner W, Hinterdorfer P, Ness W, Raab A, Vestweber D, et al. 2000. Cadherin interaction probed by atomic force microscopy. *Proc. Natl. Acad. Sci. USA* 97:4005–10
4. Bell GI. 1978. Models for the specific adhesion of cells to cells. *Science* 200:618–27
5. Binning G, Quate CF, Gerber CH. 1986. Atomic force microscope. *Phys. Rev. Lett.* 56:930–33
6. Block SM. 1995. One small step for myosin. *Nature* 378:132–33
7. Clausen-Schaumann H, Rief M, Tolksdorf C, Gaub HE. 2000. Mechanical stability of single DNA molecules. *Biophys. J.* 78:1997–2007
8. Cluzel P, Lebrun A, Heller C, Lavery R, Viovy J-L, et al. 1996. DNA: an extensible molecule. *Science* 271:792–94
9. Essevaz-Roulet B, Bockelmann U, Heslot F. 1997. Mechanical separation of complementary strands of DNA. *Proc. Natl. Acad. Sci. USA* 94:11935–40
10. Evans E. 1998. Energy landscapes of biomolecular adhesion and receptor anchoring at interfaces explored with dynamic force spectroscopy. *Faraday Discuss. Chem. Soc.* 111:1–16
11. Evans E, Leung A, Hammer D, Simon S. 2000. Chemically-distinct transition states govern rapid dissociation of single L-selectin bonds under force. *Proc. Natl. Acad. Sci. USA* In press
12. Evans E, Ludwig F. 2000. Dynamic strengths of molecular anchoring and material cohesion in fluid biomembranes. *J. Phys. Condens. Matter* 12:A315–20
13. Evans E, Ritchie K. 1997. Dynamic strength of molecular adhesion bonds. *Biophys. J.* 72:1541–55
14. Evans E, Ritchie K. 1999. Strength of a weak bond connecting flexible polymer chains. *Biophys. J.* 76:2439–47
15. Evans E, Ritchie K, Merkel R. 1995. Sensitive force technique to probe molecular adhesion and structural linkages at biological interfaces. *Biophys. J.* 68:2580–87
16. Finer JT, Simmons RM, Spudich JA. 1994. Single myosin molecule mechanics:

- piconewton forces and nanometer steps. *Nature* 368:113–19
17. Fritz J, Katopodis AG, Kolbinger F, Anselmetti D. 1998. Force mediated kinetics of single P-selectin/ligand complexes observed by atomic force microscopy. *Proc. Natl. Acad. Sci. USA* 95:12283–88
 18. Grandbois M, Beyer M, Rief M, Clausen-Schaumann H, Gaub HE. 1999. How strong is a covalent bond? *Science* 283:1727–30
 19. Grubmuller H, Heymann B, Tavan P. 1996. Ligand binding: molecular mechanics calculation of the streptavidin-biotin rupture force. *Science* 271:997–99
 20. Hanggi P, Talkner P, Borkovec M. 1990. Reaction-rate theory: fifty years after Kramers. *Rev. Mod. Phys.* 62:251–342
 21. Harada Y, Funatsu T, Murakami K, Nonoyama Y, Ishihama A, Yanagida T. 1999. Single molecule imaging of RNA polymerase-DNA interactions in real time. *Biophys. J.* 76:709–15
 22. Heymann B, Grubmuller H. 2000. Dynamic force spectroscopy of molecular adhesion bonds. *Phys. Rev. Lett.* 84:6126–29
 23. Howard J. 1998. Molecular motors: structural adaptations to cellular functions. *Nature* 389:561–66
 24. Hunt AJ, Gittes F, Howard J. 1994. The force exerted by a single kinesin molecule against a viscous load. *Biophys. J.* 67:766–81
 25. Izrailev S, Stepaniants S, Balsera M, Oono Y, Schulten K. 1976. Molecular dynamics study of unbinding of the avidin-biotin complex. *Biophys. J.* 72:1568–81
 26. Kellermayer MSZ, Smith SB, Granzier HL, Bustamante C. 1997. Folding-unfolding transitions in single titin molecules characterized with laser tweezers. *Science* 276:1112–16
 27. Kramers HA. 1940. Brownian motion in a field of force and the diffusion model of chemical reactions. *Physica* 7:284–304
 28. Kuo SC, Sheetz MP. 1993. Force of single kinesin molecules measured with optical tweezers. *Science* 260:232–34
 29. Lu H, Schulten K. 1999. Steered molecular dynamics simulations of force-induced protein domain unfolding. *Proteins: Struct. Funct. Genet.* 35:453–63
 30. Ludwig F, Evans E. 2000. How strong is molecular anchoring in biomembranes? *BIF Futura* 15:96–103
 31. Marrink S-J, Berger O, Tieleman P, Jahnig F. 1998. Adhesion forces of lipids in a phospholipid membrane studied by molecular dynamics simulations. *Biophys. J.* 74:931–43
 32. Marszalek PE, Lu H, Li H, Carrion-Vazquez M, Oberhauser AF, et al. 1999. Mechanical unfolding intermediates in titin molecules. *Nature* 402:100–3
 33. Marszalek PE, Oberhauser AF, Pang Y-P, Fernandez JM. 1998. Polysaccharide elasticity governed by chair-boat transitions of the glucopyranose ring. *Nature* 396:661–64
 34. Merkel R, Nassoy P, Leung A, Ritchie K, Evans E. 1999. Energy landscapes of receptor ligand bonds explored with dynamic force spectroscopy. *Nature* 397:50–53
 35. Meyhofer E, Howard J. 1995. The force generated by a single kinesin molecule against an elastic load. *Proc. Natl. Acad. Sci. USA* 92:574–78
 36. Oberhauser AF, Marszalek PE, Erickson HP, Fernandez JM. 1998. The molecular elasticity of the extracellular matrix protein tenascin. *Nature* 393:181–85
 37. Rief M, Gautel M, Osterhelt F, Fernandez JM, Gaub HE. 1997. Reversible unfolding of individual titin immunoglobulin domains by AFM. *Science* 276:1109–12
 38. Rief M, Osterhelt F, Heymann B, Gaub HE. 1997. Single molecule force spectroscopy on polysaccharides by AFM. *Science* 275:1295–97
 39. Silvius JR, Zuckermann MJ. 1993. Interbilayer transfer of phospholipid-anchored

- macromolecules via monomer diffusion. *Biochemistry* 32:3153–61
40. Simson DA, Ziemann F, Strigl M, Merkel R. 1998. Micropipet-based piconforce transducer: indepth analysis and experimental verification. *Biophys. J.* 74:2080–88
 41. Smith SB, Cui Y, Bustamante C. 1996. Over stretching B-DNA: the elastic response of individual double-stranded and single-stranded DNA molecules. *Science* 271:795–99
 42. Strick TR, Allemand JF, Bensimon D, Bensimon A, Croquette V. 1996. The elasticity of a single supercoiled DNA molecule. *Science* 271:1835–37
 43. Strick TR, Allemand JF, Bensimon D, Croquette V. 1998. The behavior of supercoiled DNA. *Biophys. J.* 74:2016–28
 44. Strick TR, Croquette V, Bensimon D. 1998. Homologous pairing in stretched supercoiled DNA. *Proc. Natl. Acad. Sci. USA* 95:10579–83
 45. Strick TR, Croquette V, Bensimon D. 2000. Single-molecule analysis of DNA uncoiling by a type II topoisomerase. *Nature* 404:901–4
 46. Strunz T, Oroszlan K, Shafer R, Guntherodt H-J. 1999. Dynamic force spectroscopy of single DNA molecules. *Proc. Natl. Acad. Sci. USA* 96:11277–82
 47. Svoboda K, Schmidt CF, Schnapp BJ, Block SM. 1993. Direct observations of kinesin stepping by optical trapping interferometry. *Nature* 256:721–27
 48. van Kampen NG. 1992. *Stochastic Processes in Physics and Chemistry*. Amsterdam: North-Holland. 465 pp.
 49. Wang H, Oster G. 1998. Energy transduction in the F1 motor of ATP synthase. *Nature* 396:279–82
 50. Wang MD, Schnitzer MJ, Yin H, Landick R, Gelles J, Block SM. 1998. Force and velocity measured for single molecules of RNA polymerase. *Science* 282:902–7
 51. Yin H, Wang MD, Svoboda K, Landick R, Block SM, Gelles J. 1995. Transcription against an applied force. *Science* 270:1653–56